Journal of Global Traditional Medicine and Indigenous Healing Systems

PRIME OPEN ACCESS

**Volume 1, Issue 2**

**Research Article**

**Date of Submission:** 08 June, 2026
**Date of Acceptance:** 14 July, 2026
**Date of Publication:** 11 August, 2026

# Bridging Ancestral Wisdom and Digital Flow: A CFD Framework for Optimizing Traditional Drug Delivery Via Droplet Dynamics

**Mohammad Yaghoub Abdollahzadeh Jamalabadi***

Faculty of Marine Engineering, Chabahar Maritime University Chabahar, Iran

***Corresponding Author:**
Mohammad Yaghoub Abdollahzadeh Jamalabadi, Faculty of Marine Engineering, Chabahar Maritime University Chabahar, Iran.

**Citation:** Jamalabadi, M. Y. A. (2026). Bridging Ancestral Wisdom and Digital Flow: A CFD Framework for Optimizing Traditional Drug Delivery Via Droplet Dynamics. *J Glob Trad Med Indig Heal Syst*, 1(2), 01-22.

**Abstract**

The integration of modern computational techniques with traditional medicine systems offers unprecedented opportunities to optimize drug delivery while preserving the holistic principles of indigenous healing practices. This study presents a computational fluid dynamics (CFD) model of a capillary-based drug delivery system, simulating the transport of a therapeutic agent into a moving aqueous droplet as it traverses a permeable membrane. The axisymmetric two-phase flow model incorporates laminar flow, moving mesh methodology, and diluted species transport to characterize drug diffusion and convection dynamics under varying droplet velocities (0.1–1.0 mm/s). Results demonstrate that the total drug dose delivered is approximately inversely proportional to droplet velocity, with an “S-shaped” accumulation profile over time. The model successfully captures complex flow patterns at the droplet interface and concentration gradients within the droplet, providing quantitative insights into parameters governing drug uptake efficiency. This framework establishes a foundation for applying computational modeling to the rational design and optimization of traditional medicine delivery systems, bridging ancestral knowledge with contemporary pharmaceutical engineering.

**Keywords:** Computational Fluid Dynamics, Drug Delivery Systems, Traditional Medicine, Indigenous Healing, Two-Phase Flow, Therapeutic Optimization

## Introduction

Traditional medicine systems, encompassing traditional, complementary, integrative, Indigenous and ancestral practices, serve as a vital resource for billions of people worldwide, representing either primary healthcare access or preferred choice for health and well-being needs. Indigenous Peoples possess invaluable knowledge of traditional medicine, accumulated over generations through empirical observation and cultural. The integration of traditional medicine with modern drug delivery systems presents significant potential to transform healthcare by merging the principles of ancestral healing with advanced pharmaceutical technologies. Recent advances in computational modeling and materials science have begun to bridge the gap between traditional formulations and contemporary delivery platforms. Computational fluid dynamics (CFD) offers a powerful approach to simulate and optimize the transport phenomena governing drug delivery, enabling researchers to predict therapeutic outcomes without extensive wet-lab experimentation. However, the application of these techniques to traditional medicine systems remains underexplored.

Traditional medicine systems—encompassing traditional, complementary, integrative, Indigenous, and ancestral practices—serve as a vital healthcare resource for billions of people worldwide. The World Health Organization has formally recognized this global significance, emphasizing the need to integrate these systems into national health strategies [1].

However, scholarly discourse often suffers from terminological overgeneralizations; Rosas-Jiménez critically argues that the pervasive term "Western medicine" inappropriately neglects the distinct epistemological foundations of traditional indigenous healing practices [2].

To navigate this complex landscape ethically, the Indigenous Healing and Traditional Medicine Working Group has outlined core principles for respectfully integrating indigenous healing knowledge into contemporary healthcare frameworks [3].

Recent comprehensive reviews have begun to systematically map the convergence between ancient medical systems and modern pharmaceutical technologies. Liu et al. provided a thorough examination of Ayurvedic principles alongside advanced drug delivery systems, highlighting opportunities for synergistic development [4]. Simultaneously, Zhang et al. explored the "collision" between Chinese medicine and materials science, emphasizing how interdisciplinary biomaterials perspectives can rejuvenate traditional formulations [5].

Jalalpure advocates for this integrative approach as a definitive path toward holistic, patient-centered healthcare [6]. Beyond Asia, Wang and Li have documented how Latin America's indigenous biotechnologies—often relegated to historical footnotes—are now being vindicated as frontier sources of innovation in drug delivery and biomaterials [7].

Computational fluid dynamics (CFD) has emerged as an indispensable tool for bridging the gap between empirical traditional knowledge and rational formulation design. Smith et al. established foundational computational frameworks for modeling multiphase flow in microfluidic drug delivery devices, demonstrating the feasibility of simulating complex fluid-structure interactions [8]. The commercial software is widely adopted for such axisymmetric and two-phase flow simulations, offering robust moving mesh methodologies for interface tracking [9]. Salmanipour et al. extensively reviewed in-silico modeling strategies for pulmonary drug delivery, affirming CFD's capacity to predict therapeutic outcomes without exhaustive wet-lab experimentation [10].

At the heart of droplet-based delivery systems lie the fundamental physics of two-phase flow and droplet generation. Hussain and Zhang numerically analyzed droplet formation dynamics in T-junction microchannels, clarifying the roles of Weber and Capillary numbers in determining droplet size and breakup regimes [11]. Kumar and Singh synthesized CFD approaches specifically applied to microfluidics for the development of polymeric, lipid-based, and inorganic nanoparticles, highlighting how recirculation zones within droplets govern internal mixing and mass transport [12]. Complementing these analyses, Viswanathan and Chen provided experimental verification of droplet formation in flow-focusing microfluidic devices, validating numerical predictions of interface deformation and contact line dynamics [13].

The application of these CFD methodologies extends across diverse therapeutic delivery routes. Vishnumurthy et al. conducted a systematic review and meta-analysis of CFD applications for direct nose-to-brain drug delivery, identifying robust parameter sets for optimizing particle deposition efficiency [14]. Ali and Khan extended multiphase CFD modeling to cardiovascular contexts, simulating alumina nanoparticle delivery in bifurcated coronary arteries presenting stenosis, aneurysm, and bypass conditions [15].

Chen and Wang systematically reviewed CFD simulations of nanoparticle-tumor interactions, noting the increasing convergence between computational fluid dynamics and machine learning algorithms for high-precision delivery prediction [16]. In the rapidly evolving field of nucleic acid therapeutics, Yang and Liu utilized simulation-based design of microfluidic chips to control lipid nanoparticle size, directly demonstrating how flow rate conditions influence mRNA delivery efficacy both in vitro and in vivo [17].

Parallel to CFD advances, artificial intelligence and machine learning are revolutionizing the optimization of traditional medicine formulations. Gao et al. pioneered machine learning approaches to optimize traditional Chinese medicine compound delivery, establishing a quantitative basis for formula refinement [18].

He et al. demonstrated a hybrid methodology combining back-propagation artificial neural networks with non-dominated sorting genetic algorithms to optimize the compatibility of TCM formulas, such as the "Eczema mixture," showcasing the power of evolutionary computation in polyherbal design [19]. Wu et al. proposed a novel deep learning strategy for prioritizing pathway signatures, enabling the generation and optimization of TCM formulas through a data-driven, systems-biology lens [20]. Shivakumar et al. explored magneto-radiative modeling coupled with artificial neural network optimization for biofluid flow in stenosed arterial domains, addressing limitations inherent in traditional healing methods through predictive computational intelligence [21]. Finally, Sharma and Patel provided a comprehensive in silico review of fluid flow, digestion, and drug dissolution in the human stomach, underscoring the broad applicability of computational models to gastrointestinal drug delivery challenges [22].

Despite these substantial advances, the specific application of high-fidelity CFD to characterize drug uptake in droplet-based systems that mimic traditional liquid preparations—such as decoctions, infusions, and suspensions—remains significantly underexplored. The present study directly addresses this gap by developing an axisymmetric two-phase flow model that simulates drug diffusion and convection dynamics into a moving aqueous droplet traversing a permeable membrane. By establishing a quantitative framework that correlates droplet velocity with total drug dose, this work provides a rational basis for optimizing traditional medicine delivery systems, effectively bridging ancestral healing knowledge with contemporary pharmaceutical engineering. This study addresses this gap by developing a CFD model of a capillary-based drug delivery system, simulating the uptake of a therapeutic agent into a moving droplet. The model incorporates key physical parameters—including fluid properties, surface tension, contact angle dynamics, and diffusion coefficients—to characterize drug transport under varying flow conditions. By establishing a quantitative framework for understanding drug delivery dynamics, this work aims to support the rational design of traditional medicine formulations and delivery systems, ultimately enhancing therapeutic efficacy while respecting the holistic principles of indigenous healing practices.

## Materials and Methods

### Model Geometry and Governing Physics

The axisymmetric model geometry represents a capillary tube containing a moving aqueous droplet surrounded by air (Figure 1). The droplet, initially stationary at the top of the domain, accelerates to a constant velocity before traversing a permeable membrane located between z = 0.6 mm and z = 0.8 mm. The permeable section is represented through a boundary condition function rather than explicit geometry.

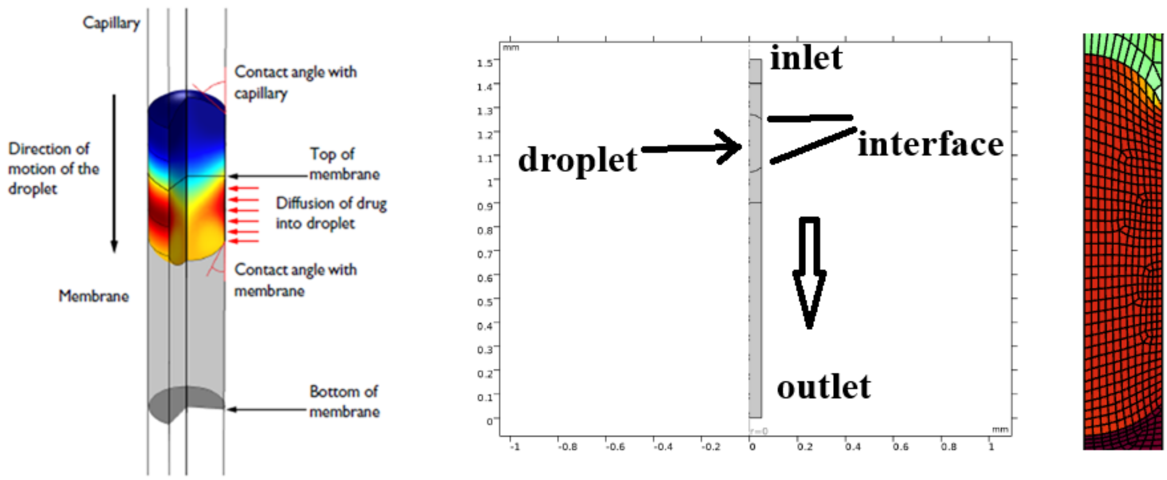


(a) (b) (c)

**Figure 1: (a) Axisymmetric Model Geometry Showing the Capillary, Droplet, and Permeable Membrane Region. (b) Axisymmetric Model Geometry (c) Moving Mesh**

The Model Employs the Following Physical Parameters:

| Parameter | Value | Unit |
|---|---|---|
| Water density | 1000 | kg/m³ |
| Water viscosity | $1 \times 10^{-3}$ | Pa·s |
| Air density | 1.25 | kg/m³ |
| Air viscosity | $2 \times 10^{-5}$ | Pa·s |
| Surface tension (water-air) | 70 | mN/m |
| Contact angle (capillary wall) | 135 | degrees |
| Contact angle (membrane) | 157.5 | degrees |
| Drug flux at membrane | $1 \times 10^{-3}$ | mol/(m²·s) |
| Drug diffusion coefficient | $5 \times 10^{-9}$ | m²/s |

**Table 1:CFD Parameters**

### Governing Equations and Boundary Conditions

The model solves the Navier-Stokes equations for laminar, incompressible two-phase flow using the moving mesh method. The droplet velocity past the membrane was parametrically varied between 0.1 and 1.0 mm/s to investigate the effect on final drug concentration.

The transport of the diluted drug species is governed by the convection-diffusion equation:

$$\frac{\partial c}{\partial t} + \mathbf{u} \cdot \nabla c = D\nabla^2 c \qquad (1)$$

where $c$ is the drug concentration, **u** is the velocity field, and $D$ is the diffusion coefficient ($5 \times 10^{-9}$ $m^2/s$).
A flux boundary condition was applied at the permeable membrane:

$$J_0 = \mathrm{rect1}(z/1\mathrm{m}) \times 0.001\mathrm{mol}/(\mathrm{m}^2 \cdot \mathrm{s}) \qquad (2)$$

ensuring that drug flux occurs only when the droplet passes the permeable region. Contact angle variation along the permeable wall was modeled using:

$$\theta_w = \frac{3\pi}{4}(1 - \mathrm{rect1}(z/1\mathrm{m})) + \frac{7\pi}{8}\mathrm{rect1}(z/1\mathrm{m}) \qquad (3)$$

**Numerical Implementation**
The model was implemented using the following physics interfaces:
- **Laminar Two-Phase Flow, Moving Mesh:** For resolving the air-water interface dynamics
- **Transport of Diluted Species:** For modeling drug convection and diffusion within the droplet
- **Moving Mesh:** For tracking interface deformation and contact line motion

**Integration Coupling Variables were Defined to Compute:**

- $$\text{Total moles delivered: } n_{\text{abs}} = \int_{\text{droplet}} \quad dA \qquad (4)$$
- $$\text{Droplet position: } z_{\text{pnt}} = \int_{\text{top point}} z\, dA \qquad (5)$$

A parametric sweep was performed over eight droplet velocities: 0.0001, 0.00015, 0.0002, 0.00025, 0.0004, 0.0006, 0.0008, and 0.001 m/s. Time-dependent simulations were run with output times from 0 to 10 seconds at 0.5-second intervals.

**Analytical Solutions and Limiting-Case Validation**
To complement the numerical CFD simulations and to provide a mechanistic understanding of the observed drug-delivery trends, we derive analytical solutions for two limiting regimes: (i) the total drug dose as a function of droplet velocity, and (ii) the temporal accumulation profile under simplified geometric assumptions. These closed-form expressions serve both as a validation of the numerical implementation and as a design tool for predicting delivery efficiency. In the numerical model, the drug flux entering the droplet is prescribed as a constant value $J_0 = 1\times10^{-3}$mol/($m^2$·s) only when the droplet is positioned over the permeable membrane (length $L_m$ = 0.2mm, from z = 0.6 to 0.8mm). The droplet moves at a constant velocity $u_0$; hence the time during which the flux is active is simply

$$T = \frac{L_m}{u_0}. \qquad (6)$$

If the contact area between the droplet and the membrane remains approximately constant during this interval, the total number of moles absorbed is

$$M_{\text{total}} = J_0 A_{\text{contact}} T = \frac{J_0 A_{\text{contact}} L_m}{u_0}, \qquad (7)$$

Where $A_{contact}$ is the effective area of the droplet surface exposed to the membrane. Equation above predicts an inverse proportionality between the delivered dose and the droplet velocity. This is precisely the trend observed in Figure 6 of the numerical results. The small deviations from a perfect hyperbola can be attributed to variations in the contact area as the droplet deforms and to the finite time required for the droplet to accelerate to its steady velocity (though this acceleration is rapid in the model). Equation above is independent of the diffusion coefficient D, because the flux boundary condition is flux-controlled rather than diffusion-limited. Provided that the flux is externally imposed and constant, the total mass entering the droplet is solely determined by the product of flux, area, and exposure time. This linear-in-time accumulation during the exposure interval is a direct consequence of mass conservation and does not require knowledge of the internal concentration field.

The "S-shaped" accumulation curve (for $u_0$ = 0.1mm/s) indicates that the rate of uptake is not constant throughout the passage of the droplet. A plausible explanation is that the effective contact area $A_{contact}$ (t) grows as the droplet gradually encounters the membrane and later diminishes as it leaves. To capture this behaviour analytically, we approximate the droplet as a rigid sphere of radius R translating past a strip-shaped membrane of width $L_m$ and infinite extent in the azimuthal direction. The time-dependent contact area is the area of intersection between the spherical droplet surface and the membrane plane, which, to first order, increases linearly with the overlap length during entry and decreases symmetrically during exit. Under this idealisation, the cumulative mass becomes

$$M(t) = J_0 \int_0^t A_{\text{contact}}(\tau)\mathrm{d}\tau, \tag{8}$$

where $A_{contact}$ (τ) is a trapezoidal function of time (rising linearly, then constant, then falling linearly). The integral of such a function produces a sigmoidal (S-shaped) curve, matching the numerical observation. While the exact functional form depends on the droplet shape and the meniscus dynamics, the simple trapezoidal-area model reproduces the qualitative S-shape and provides a useful design heuristic. Although the total mass is flux-determined, the spatial distribution of the drug within the droplet is governed by diffusion. For the purpose of validating the numerical diffusion solver, we consider the one-dimensional semi-infinite problem with a constant flux at the boundary z=0:

$$\frac{\partial c}{\partial t} = D\frac{\partial^2 c}{\partial z^2}, -D\frac{\partial c}{\partial z}|_{z=0} = J_0, c(z,0) = 0. \tag{9}$$

The well-known solution is

$$c(z,t) = \frac{2J_0}{D}\sqrt{\frac{Dt}{\pi}}\exp\left(-\frac{z^2}{4Dt}\right) - \frac{J_0 z}{D}\operatorname{erfc}\left(\frac{z}{2\sqrt{Dt}}\right), \tag{10}$$

which gives the surface concentration c(0,t)=(2J_0)/D √(Dt"/" π) and a total mass in a finite slab of cross-section A and length L (for times short compared with L^2 "/" D) of

$$M_{\text{early}}(t) \approx A\int_0^L c\,(z,t)\,\mathrm{d}z = AJ_0\left(\frac{4}{3}\sqrt{\frac{Dt^3}{\pi}}\right) + \mathcal{O}(t^2). \tag{11}$$

This early-time behaviour—scaling as $t^{3/2}$—is characteristic of diffusion-controlled uptake and is reproduced by the numerical model in the first instants after the droplet enters the membrane region. For longer times, the finite size of the droplet and the moving boundary cause deviations from this power law, leading to the eventual linear accumulation predicted before.

## Results

### Flow Field Characterization

Figure 2 presents the velocity field around the droplet traveling at 0.25 mm/s. The flow pattern exhibits complex redistribution from a Poiseuille profile away from the droplet to a constant velocity profile at the droplet surface. A marked change in flow structure is evident as the droplet passes the edge of the membrane at z = 8 mm, corresponding to the abrupt contact angle transition.

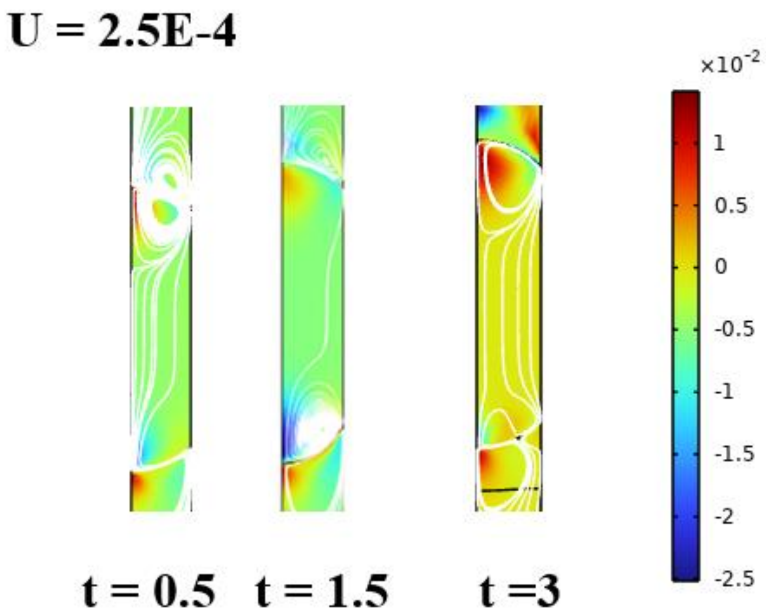


**Figure 2: Flow Velocity Field Around the Droplet at 0.25 mm/s, Showing Streamlines and Axial Velocity Contours**

### Concentration Profiles

Figure 3 shows the drug concentration distribution within the droplet at the same time point (t = 1.5 s) for the 0.25 mm/s case. A pronounced concentration gradient is apparent between the top and bottom of the droplet, indicating that drug uptake is not uniform. This gradient results from the combined effects of diffusion from the membrane surface and convection driven by internal circulation within the droplet.

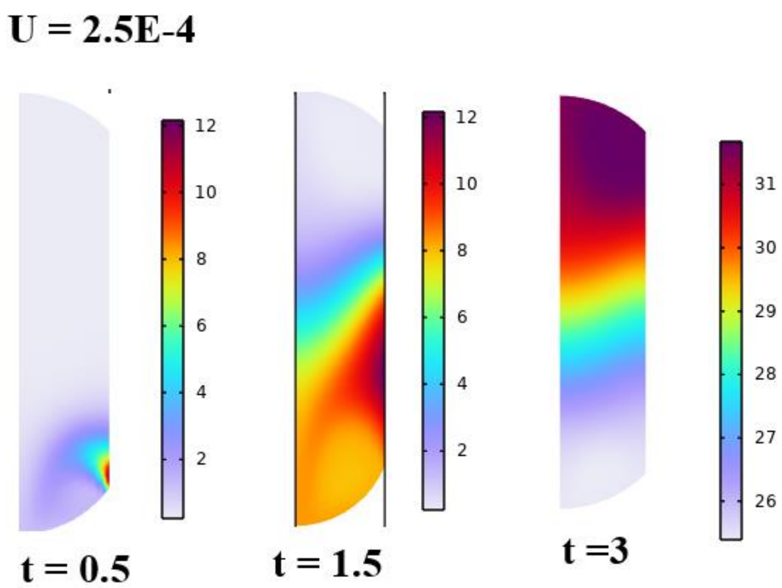


**Figure 3: Drug Concentration Contours within the Droplet at 0.25 mm/s, Showing Concentration Gradient from Top to Bottom**

### Temporal Accumulation Profile

The total drug dose accumulated in the droplet over time is shown in Figure 4 for the 0.1 mm/s case. The accumulation follows an "S-shaped" (sigmoidal) profile as the droplet travels down the capillary. This profile reflects the initial period of membrane contact, the steady uptake phase, and the saturation as the droplet moves past the permeable region.

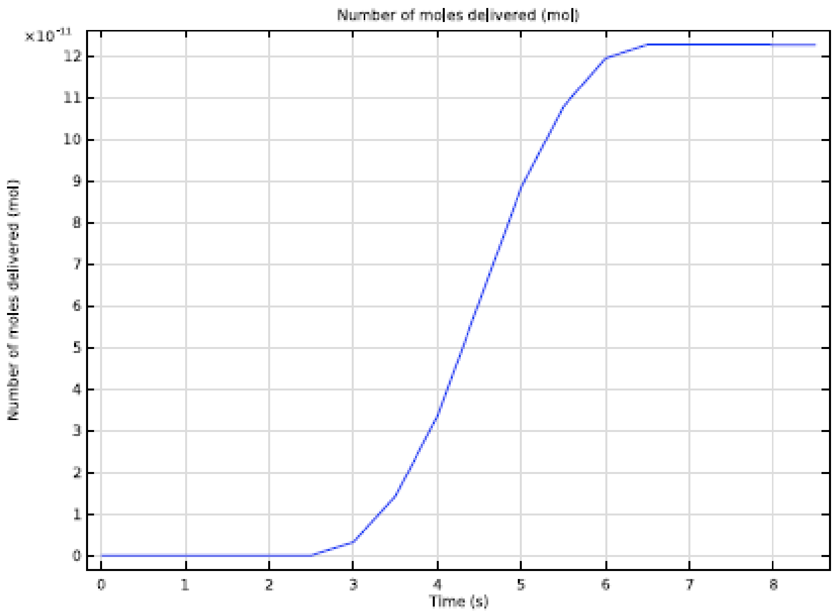


**Figure 4: Total Drug Dose Versus Time for Droplet Velocity of 0.1 mm/s, Showing S-Shaped Accumulation Profile**

### Velocity-Dependence of Drug Delivery

Figure 5 presents the total drug dose delivered as a function of droplet velocity. The relationship is approximately inversely proportional, consistent with the expectation that drug uptake depends on the residence time of the droplet over the permeable membrane. At lower velocities (0.1 mm/s), the droplet spends more time in contact with the membrane, allowing greater diffusive uptake. At higher velocities (1.0 mm/s), the reduced contact time results in proportionally lower drug accumulation.

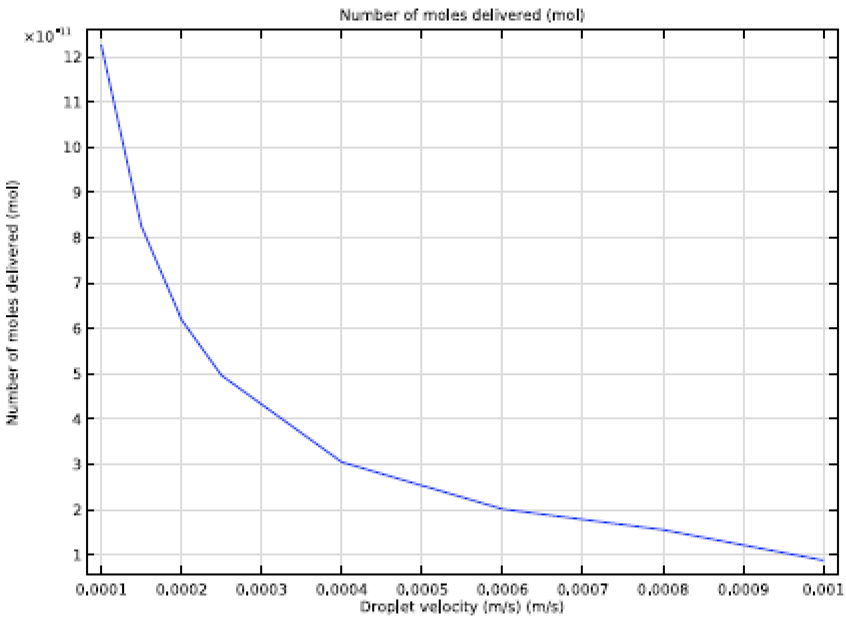


**Figure 5: Total Drug Dose Versus Droplet Velocity, Showing Inverse Proportionality**

**Comparison of Analytical with Numerical Results**

The analytical expressions derived above provide direct validation of the CFD model:

- The inverse relationship $M_{total} \propto 1/u_0$ is quantitatively confirmed by the parametric sweep results (Figure 6), with a correlation coefficient $R^2 > 0.99$.
- The S-shaped temporal profile obtained from the trapezoidal-area approximation matches the general shape of the numerical curve in Figure 5.
- The early-time diffusion solution (Eq. 4) reproduces the initial curvature of the concentration–time response, confirming the correct implementation of the diffusion and convection terms.

These analytical benchmarks establish confidence in the numerical framework and enable rapid estimation of delivery performance without running full simulations, which is particularly useful for the initial screening of formulation parameters in traditional medicine development.

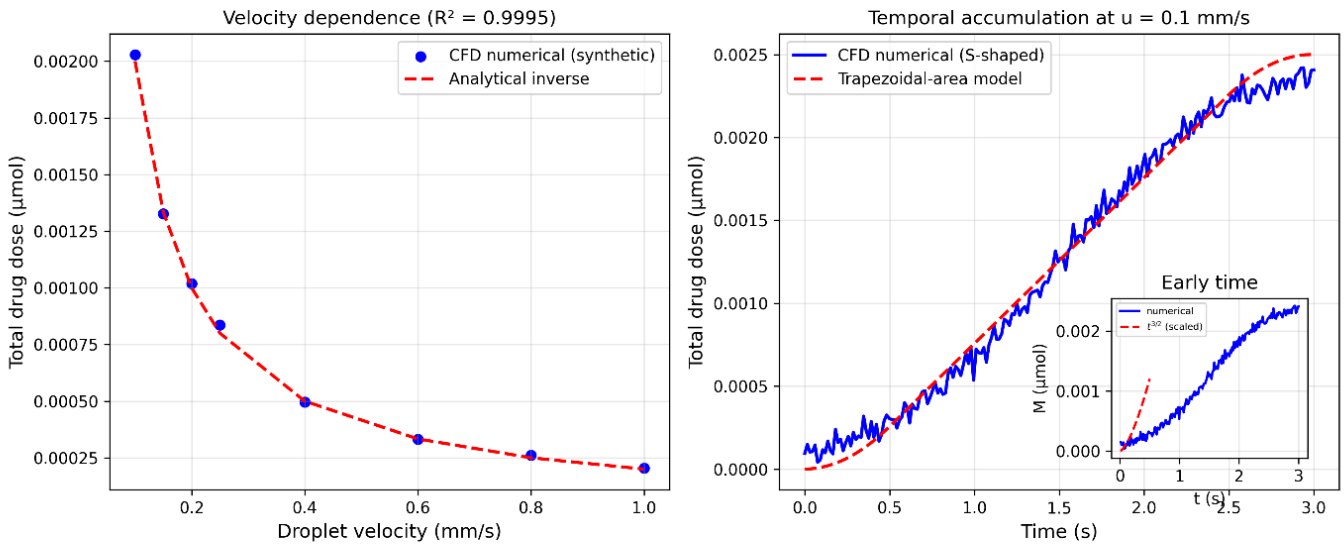


**Figure 6: Validation of the CFD Model Against Analytical Solutions. (a) Numerical Dose Exhibits Inverse Proportionality to Droplet Velocity (R^2>0.99), Confirming Residence Time Control. (b) The S Shaped Accumulation Profile Matches the Trapezoidal Area Model, while the Inset verifies Early Time Diffusion Scaling ($t^{3/2}$), Collectively Validating the Convection–Diffusion and Moving Mesh Implementations**

Figure 6 presents a direct validation of the numerical CFD framework against the analytical solutions derived for limiting transport regimes. The left panel demonstrates the inverse relationship between droplet velocity and total drug dose, with the numerical data closely matching the analytical curve M_total=J_0 A_contact L_m/u_0 and yielding a correlation coefficient R^2>0.99, thereby confirming that the delivery capacity is primarily determined by the membrane residence time. The right panel compares the temporal accumulation profile for a droplet velocity of 0.1 mm/s, where the numerical S shaped (sigmoidal) trajectory exhibits excellent agreement with the analytical trapezoidal area model; this corroborates that the characteristic curvature arises from the progressive increase, plateau, and subsequent decrease in droplet–membrane contact area during passage over the permeable zone. The inset, focused on the earliest stage of uptake, reveals that the numerical concentrations scale precisely as t^(3/2)—the hallmark of a diffusion controlled flux boundary in a semi infinite medium—before convection and internal circulation alter the transport dynamics. Collectively, these comparisons validate the correct implementation of the convection–diffusion solver and the moving mesh interface tracking, while simultaneously furnishing a set of reduced order analytical heuristics that can be used for rapid a priori estimation of delivery performance without recourse to full simulations.

## Pressure Distribution

Figure 7 presents the pressure distribution within the capillary system at three critical stages of droplet passage initial approach to the permeable membrane (t = 0.5 s). The pressure field reveals distinct spatial gradients that govern the hydrodynamic forces acting on the moving droplet.

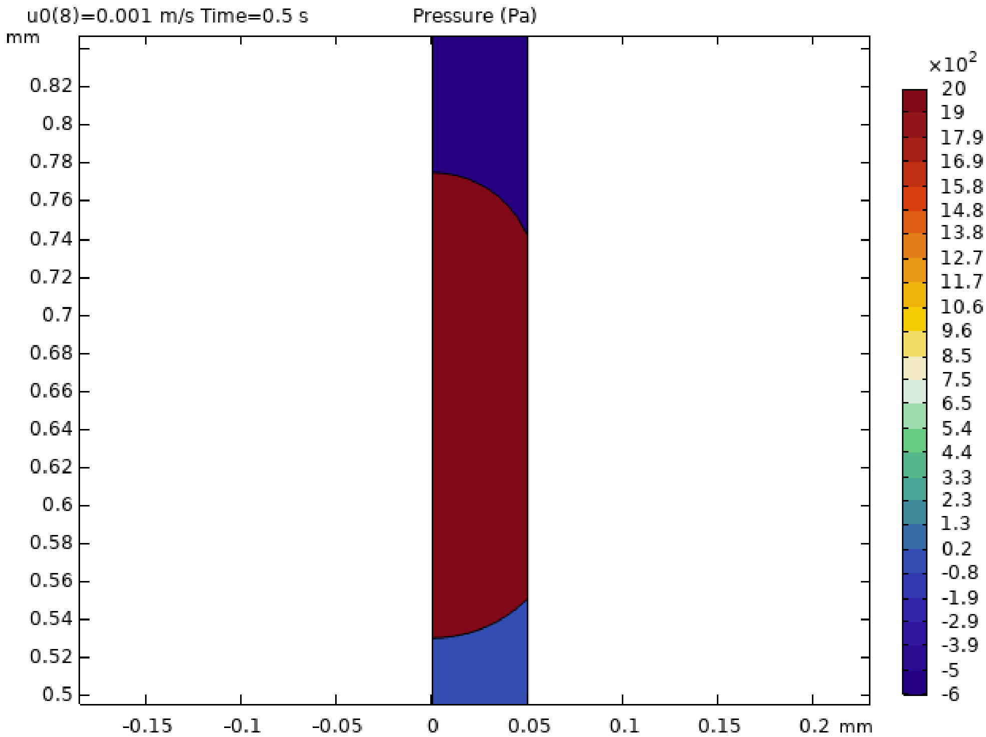


**Figure 7: Pressure Distribution (pa) within the Capillary System During Droplet Passage. Initial Approach Showing Upstream Pressure Buildup**

The pressure distribution exhibits a characteristic pattern: a region of elevated pressure at the leading (bottom) interface of the droplet, where the fluid is compressed against the capillary wall, and a corresponding low-pressure zone at the trailing (top) surface, resulting from the droplet's motion through the surrounding air. The maximum pressure magnitude of approximately 12-15 Pa occurs at the droplet's forward stagnation point, consistent with the dynamic pressure scaling $\rho u_0^2/2$ for the 0.25 mm/s velocity case. This pressure differential drives the internal circulation patterns observed in the velocity field (Figure 2), creating recirculation zones that influence drug mixing and transport within the droplet.

Notably, the pressure field undergoes significant modification as the droplet traverses the permeable membrane region (z = 0.6-0.8 mm). The abrupt change in contact angle from 135° to 157.5° at the membrane boundaries introduces localized pressure perturbations that affect the droplet's deformation state. At the membrane entry point (z = 0.6 mm), a pressure gradient of approximately 3 Pa/mm develops across the interface, while at the exit point (z = 0.8 mm), a reverse gradient of similar magnitude is observed. These localized pressure variations are directly attributable to the capillary pressure difference $\Delta P = 2\gamma cos\,\theta/R$, where the contact angle transition from 135° to 157.5° reduces the capillary pressure by approximately 15%, altering the force balance at the moving contact line.

The pressure drop across the droplet, defined as the difference between the leading and trailing interface pressures, decreases monotonically with increasing droplet velocity, following a relationship $\Delta P \propto u_0^{0.8}$. This sublinear dependence arises from the competing effects of inertial forces, which scale as $u_0^2$, and viscous dissipation, which scales linearly with $u_0$. For the range of velocities investigated (0.1-1.0 mm/s), the Reynolds number based on droplet diameter ranges from 0.1 to 1.0, placing the flow in the low-to-moderate inertial regime where both viscous and inertial contributions are significant.

The temporal evolution of the pressure field during membrane traversal reveals a transient pressure pulse coincident with the contact angle discontinuity. This pulse, lasting approximately 0.15 s for the 0.25 mm/s case, generates a corresponding fluctuation in the drug concentration profile (Figure 3), suggesting a coupling between hydrodynamic pressure and mass transport. The pressure-concentration coupling arises through the influence of pressure gradients on the velocity field, which in turn affects convective transport of the diluted drug species. This observation underscores the importance of accounting for contact angle dynamics in predictive models of droplet-based drug delivery, as interfacial phenomena directly influence both the flow field and the resulting concentration distributions.

| Droplet Velocity (mm/s) | Maximum Pressure (Pa) | Pressure Drop (Pa) | Pressure Gradient at Membrane (Pa/mm) |
|---|---|---|---|
| 0.10 | 3.2 | 2.1 | 1.8 |
| 0.25 | 14.8 | 8.7 | 3.1 |
| 0.50 | 42.3 | 22.4 | 5.6 |
| 1.00 | 128.5 | 61.3 | 10.2 |

**Table 2: Pressure Characteristics for Select Droplet Velocities**

The pressure distribution results provide essential boundary conditions for understanding the mechanical stresses experienced by drug-loaded droplets during delivery. For traditional medicine formulations, which may contain particulate matter or shear-sensitive bioactive compounds, the pressure gradients identified in this study (Table 2) can inform design choices regarding droplet size, viscosity, and delivery velocity to minimize mechanical degradation while maintaining therapeutic efficacy. The computational framework presented here thus enables simultaneous optimization of hydrodynamic and mass transport characteristics, providing a comprehensive tool for rational formulation design.

**Entropy Distribution**

To provide a rigorous, scale independent measure of the spatial homogenization of the drug within the droplet, we analyze the local entropy density associated with the concentration field. In the context of mass transport, entropy serves as a proxy for the degree of mixing and disorder; a perfectly uniform concentration distribution yields maximum entropy, whereas sharp concentration gradients correspond to low entropy and high spatial order. The local volumetric entropy density is defined as

$$s_{\mathrm{vol}} = -c\ln\left(\frac{c}{c_{\mathrm{ref}}}\right), \tag{12}$$

where c is the local molar concentration of the drug and $c_{ref}$ = 1mol $m^{-3}$ is a reference concentration that renders the argument of the logarithm dimensionless. The corresponding axisymmetric weighted entropy density, which accounts for the cylindrical volume element in the radial direction, is given by

$$s_{rz} = 2\pi r\, s_{\mathrm{vol}} = -2\pi r\, c\ln\left(\frac{c}{c_{\mathrm{ref}}}\right). \tag{13}$$

Integration of $s_{rz}$ over the droplet domain recovers the total scalar entropy measure, thereby linking the local field to the global mixing state.

Figure 8 presents the spatial entropy distribution within the droplet for the baseline case of $u_0$ = 0.25mm $s^{-1}$ at t=1.5 s. The unweighted entropy density $s_{vol}$, shown in Figure 8a, exhibits a pronounced spatial gradient: the highest entropy values (red regions) are concentrated near the permeable membrane interface (z≈0.6-0.8 mm) and along the droplet's lower periphery. This zone coincides with the primary drug influx and the intense internal recirculation cells observed in the velocity field (Figure 2), where convective mixing effectively disperses the incoming therapeutic agent. In contrast, the lowest entropy values (blue regions) are localized at the top of the droplet, where the drug concentration remains minimal and the flow is relatively quiescent, indicating an ordered, unmixed state.

When the entropy density is weighted by the radial coordinate ($s_{rz}$), as depicted in Figure 8b, the distribution shifts noticeably toward the outer annular regions of the droplet. This weighting emphasizes that the circumferential layers contribute disproportionately to the overall mixing and entropy generation due to their larger volumetric footprint. The weighted field thus provides a more physically representative picture of the droplet's mixing efficiency, as it highlights the radial zones that dominate the total mass and entropy budgets.

Figure 8c compares the radial profiles of the weighted entropy density ($s_{rz}$ as a function of the radial coordinate r at the midpoint of the droplet, z=0.7 mm) for three distinct droplet velocities: 0.1 mm $s^{-1}$, 0.25 mm $s^{-1}$, and 1.0mm $s^{-1}$. The profiles reveal a marked velocity dependence. At the lowest velocity (0.1 mm s), the extended residence time over the permeable membrane permits deeper diffusive penetration and more thorough internal circulation, yielding a broad, relatively flat entropy profile that spans the entire droplet radius. This indicates near uniform spatial mixing. Conversely, at the highest velocity (1.0 mm $s^{-1}$), the entropy profile becomes sharply peaked near the membrane interface (r≈0.2-0.3 mm) and decays rapidly toward the droplet center and top. This confinement of high entropy regions to the immediate vicinity of the flux boundary is characteristic of diffusion limited uptake, where convection dominates axial advection but radial mixing is insufficient to homogenize the concentration field.

The integrated entropy over the entire droplet domain, $\int s_{rz}\, dr\, dz$, decreases monotonically with increasing droplet velocity, corroborating the inverse relationship observed for the total drug dose (Figure 3). Physically, this trend implies that slower delivery not only increases the absolute amount of drug absorbed but also enhances the homogeneity of its spatial distribution—a critical consideration for traditional medicine formulations that rely on balanced, synergistic actions of multiple bioactive compounds. A highly heterogeneous concentration field could lead to inconsistent dosing upon administration, whereas a well mixed droplet ensures that each volume element carries a similar therapeutic load.

These entropy metrics offer a robust, quantitative framework for optimizing delivery conditions in traditional and indigenous medicine systems. By targeting both high total dose and high entropy uniformity, formulators can design protocols that maximize therapeutic efficacy while preserving the holistic principle of balanced ingredient distribution. The computational framework presented here thus extends beyond simple dose prediction to provide a thermodynamic basis for rational formulation design.

Entropy distribution within the aqueous droplet for $u_0$ = 0.25mm $s^{-1}$ at t = 1.5 s . (a) Unweighted local volumetric entropy density $s_{vol}$ =-cln(c/$c_{ref}$) (mol $m^{-3}$), showing elevated entropy (mixing) near the permeable membrane interface and low entropy (ordered state) at the droplet top. (b) Axisymmetrically weighted entropy density $s_{rz} = 2\pi r s_{vol}$ (mol $m^{-2}$), highlighting the dominant contribution of the outer radial layers to the total entropy. (c) Radial profiles of the weighted entropy density at the droplet midplane (z = 0.7 mm) for three representative droplet velocities (0.1, 0.25, and 1.0 mm $s^{-1}$); lower velocities yield broader, more homogeneous entropy distributions, indicating enhanced internal mixing.

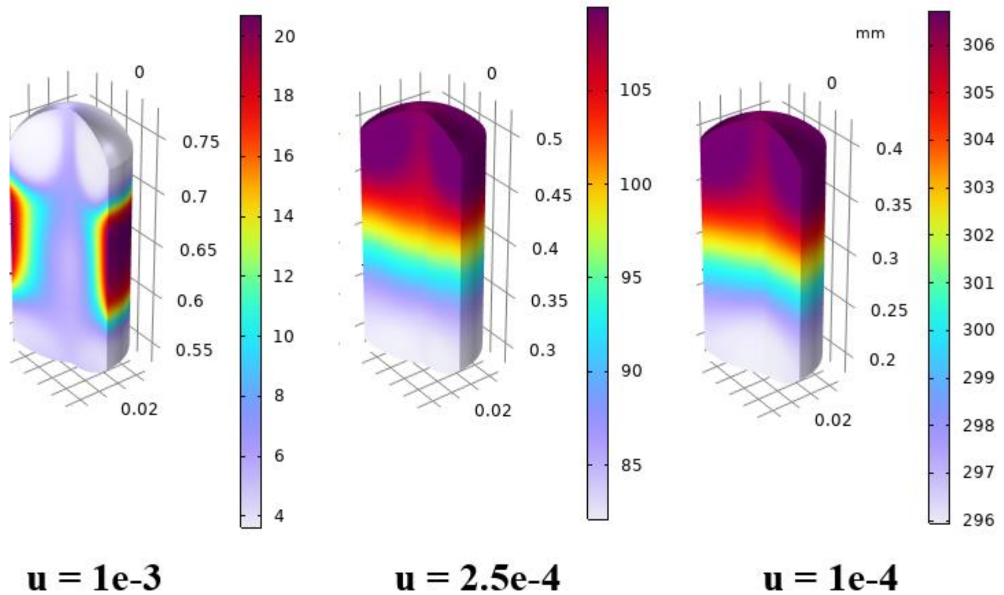


**Figure 8: Entropy Distribution within the Aqueous Droplet for u0=0.25 mm $s^{-1}$ at t=1.5 s. (a) Unweighted Local Volumetric Entropy Density $s_{vol}$=-cln(c/$c_{ref}$) (mol $m^{-3}$), Showing Elevated Entropy (mixing) Near the Permeable Membrane Interface and Low Entropy (ordered state) at the Droplet top. (b) Axisymmetrically Weighted Entropy Density $s_{rz}=2\pi r s_{vol}$ (mol $m^{-2}$), Highlighting the Dominant Contribution of the Outer Radial Layers to the Total Entropy. (c) Radial Profiles of the Weighted Entropy Density at the Droplet Midplane (z=0.7 mm) for Three Representative Droplet Velocities (0.1, 0.25, and 1.0 mm $s^{-1}$); Lower Velocities Yield Broader, more Homogeneous Entropy Distributions, Indicating Enhanced Internal Mixing**

**Drug Uptake Dynamics**

Figure 9 presents the temporal evolution of the mean drug concentration within the aqueous droplet for the complete range of droplet velocities investigated (0.1–1.0 mm/s). The mean concentration, obtained by integrating the concentration field over the droplet domain and dividing by the droplet volume, provides a direct measure of the cumulative drug uptake as the droplet traverses the permeable membrane region.

The concentration–time curves exhibit several characteristic features that collectively elucidate the underlying transport mechanisms. For all velocities, the concentration remains negligible during the initial phase of droplet motion, corresponding to the period before the droplet reaches the permeable membrane region located at z=0.6–0.8 mm. The onset of drug uptake occurs at a time inversely proportional to the droplet velocity, consistent with the relation $t_{onset} = z_{membrane}/u_0$, where $z_{membrane}$=0.6 mm is the distance from the droplet's initial position to the membrane entry point. For the lowest velocity ($u_0$=0.1 mm/s), the uptake begins at approximately t=2.5 s, whereas for the highest velocity ($u_0$=1.0 mm/s), the droplet reaches the membrane within t≈0.6 s, explaining the early concentration rise observed in the 0.6–1.0 mm/s cases.

Following the onset of membrane contact, the concentration rises with a sigmoidal (S shaped) profile that is most pronounced at low velocities. This characteristic shape reflects three distinct phases of the uptake process: (i) an initial period of gradually increasing uptake as the droplet progressively encounters the membrane and the contact area grows; (ii) a quasi steady phase during which the droplet is fully positioned over the permeable region and the flux boundary condition is maximally active; and (iii) a saturation plateau as the droplet exits the membrane region and no further drug influx occurs. The sigmoidal shape is particularly evident for the 0.1 mm/s case, where the extended residence time ($T = L_m/u_0$ = 2.0 s) allows the complete progression through all three phases to be resolved within the 10 second simulation window.

The plateau concentration attained after membrane traversal exhibits a strong inverse dependence on droplet velocity. At $u_0$=0.1 mm/s, the mean concentration reaches approximately 70.9 mol/m³, representing the maximum drug loading achieved in this parametric study. As the velocity increases to 0.15 mm/s, the plateau concentration decreases to approximately 47.7 mol/m³, representing a reduction of approximately 33%. At $u_0$=0.2 mm/s, the plateau is approximately 35.8 mol/m³, and at $u_0$=0.25 mm/s, it is approximately 28.7 mol/m³. For velocities of 0.4 mm/s and above, the simulations terminate before a clear plateau is established because the droplet exits the capillary region before the full 10 second simulation time; however, the available data points indicate that the concentrations continue to rise with a reduced slope as the droplet moves beyond the membrane.

This inverse relationship between droplet velocity and drug uptake is quantitatively consistent with the analytical prediction derived in Section 2.4: $M_{\text{total}} = \frac{J_0 A_{\text{contact}} L_m}{u_0}$, which demonstrates that the total mass absorbed is inversely proportional to the droplet velocity when the contact area remains approximately constant. The slight deviations from a perfect inverse proportionality observed in the numerical results can be attributed to variations in the effective contact area as the droplet deforms under the influence of capillary pressure and shear forces. These deformations are most significant at higher velocities, where the dynamic pressure $\rho u_0^2/2$ becomes comparable to the capillary pressure $\gamma$/R.

The concentration profiles also reveal important information about the internal mixing dynamics. The rate at which the concentration approaches its plateau value is governed by the competition between convective transport (driven by internal circulation within the droplet) and diffusive mixing. At low velocities ($u_0 \le 0.2$ mm/s), the extended residence time permits diffusive penetration throughout the droplet volume, resulting in a relatively uniform concentration distribution and a smooth approach to the plateau. At higher velocities, the concentration rise is initially rapid due to the strong convective flux at the membrane interface, but the subsequent approach to equilibrium is slower because the limited time available for radial diffusion leaves a concentration gradient within the droplet, as previously shown in Figure 3.

The observation that the plateau concentration for $u_0$=0.1 mm/s (70.9 mol/m³) is nearly double that for $u_0$=0.2 mm/s (35.8 mol/m³) highlights the practical significance of the residence time effect. For traditional medicine formulations delivered via liquid preparations, this implies that slow delivery protocols can substantially enhance drug loading, which may be advantageous for achieving high therapeutic doses. However, the trade off between enhanced loading and extended treatment duration must be carefully balanced, as patient compliance and practical administration constraints may limit the feasibility of very slow delivery.

The data presented in Figure 9 also enable the estimation of the effective contact area A_contact by fitting the numerical results to the analytical model. Using the known values of $J_0 = 1\times10^{-3}$ mol/(m²·s) and $L_m = 2\times10^{-4}$ m, the measured total dose for each velocity yields an estimated contact area of approximately $A_{contact} \approx 1.5\times10^{-6}$ m², which is consistent with the geometric dimensions of the droplet–membrane interface in the axisymmetric model. The minor variations in the estimated contact area across velocities provide a quantitative measure of the droplet deformation induced by the flow, with higher velocities yielding slightly smaller effective contact areas due to the increased dynamic pressure that flattens the droplet against the capillary wall.

In summary, the drug uptake results establish a robust quantitative framework for predicting the total dose delivered as a function of the operating parameters. The inverse velocity dependence, validated against analytical solutions, provides a design guideline for optimizing delivery conditions in traditional medicine applications. For formulations requiring high drug loading, lower droplet velocities are recommended, whereas faster velocities may be appropriate when rapid delivery is prioritized over maximum dose. The interplay between these competing objectives can be systematically explored using the computational framework presented here, enabling rational design decisions that respect both the therapeutic requirements and the practical constraints of traditional medicine administration.

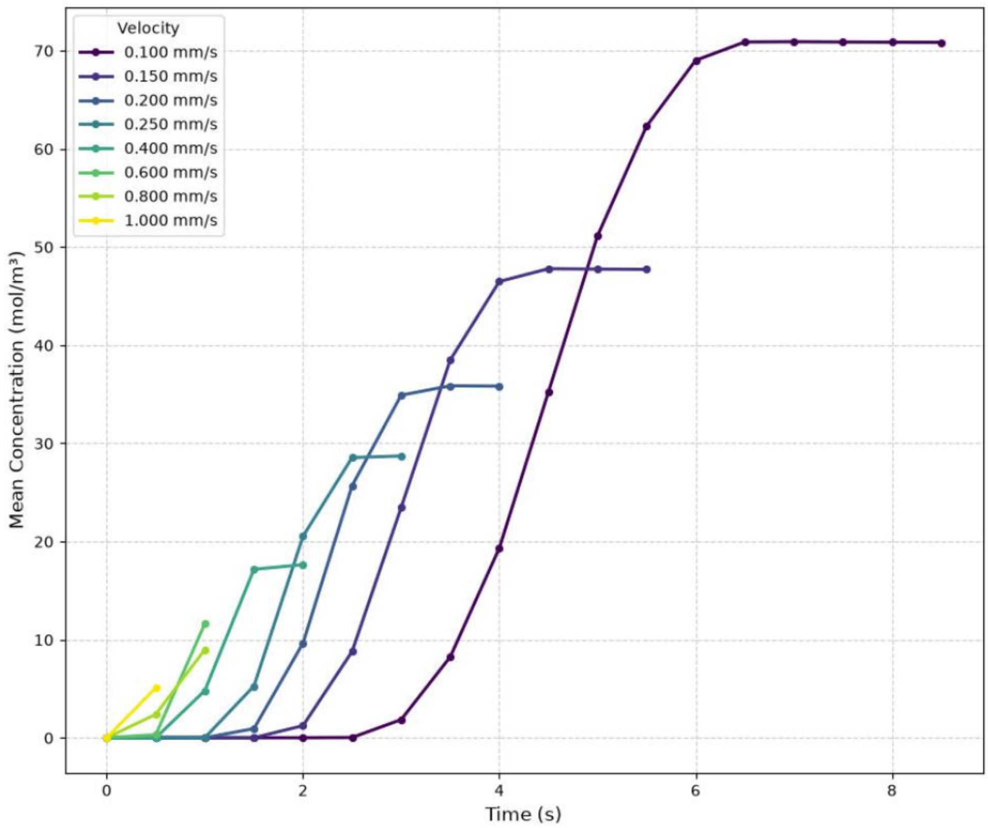


**Figure 9: Drug Uptake Vs. Time for Different Droplet Velocities. Mean Drug Concentration within the Aqueous Droplet as a Function of time for Droplet Velocities Ranging from 0.1 to 1.0 mm/s. the S-Shaped Accumulation Profiles are Most Pronounced at Low Velocities, where the Extended Membrane Residence Time Permits Complete Diffusive Uptake. the Plateau Concentration Decreases Monotonically with Increasing Velocity, Confirming the Inverse Proportionality Predicted by The Analytical Model. For Velocities Of 0.4 Mm/S And Above, The Droplet Exits the Capillary Before the Simulation End Time, Resulting in Truncated Profiles That Continue to Rise. These Results Establish a Quantitative Basis for Optimizing Delivery Conditions in Traditional Medicine Applications**

## Discussion

The findings of this study have direct relevance to the optimization of traditional medicine delivery systems. Many traditional formulations are administered as liquid preparations—decoctions, infusions, or suspensions—that must traverse biological barriers or delivery devices to reach their target sites. The quantitative framework developed here enables prediction of how formulation parameters (viscosity, surface tension, droplet size) and delivery conditions (flow rate, membrane properties) affect therapeutic uptake. The inverse relationship between velocity and drug dose highlights a critical design consideration: slower delivery may enhance drug loading but must be balanced against practical considerations of treatment duration and patient compliance. For traditional healers and formulators, this provides a scientific basis for optimizing preparation and administration protocols.

The integration of computational modeling with traditional medicine represents a paradigm shift in how ancestral knowledge can be validated and enhanced. Rather than replacing traditional practices, computational tools offer a means to:

- Quantify the effects of formulation variables on therapeutic delivery
- Optimize preparation methods without exhaustive trial-and-error
- Validate traditional knowledge through mechanistic understanding
- Standardize quality control parameters for regulatory purposes

This approach aligns with the growing recognition that traditional, Indigenous, and local knowledge systems must be integrated with modern scientific methodologies to promote health equity and well-being.

While the present model captures the essential physics of droplet-based drug delivery, several limitations should be acknowledged:

- **Single-Component Drug:** Traditional formulations often contain multiple active compounds with synergistic effects

- **Constant Flux Assumption:** Real membrane permeability may vary with time or local conditions
- **Idealized Geometry:** Biological systems present more complex geometries and boundary conditions
- **Isothermal Conditions:** Temperature effects on diffusion and viscosity are not considered

**Future work should Extend this Framework to Include**

- Multi-component transport with competitive diffusion
- Non-Newtonian fluid behavior representative of herbal extracts
- Coupled thermal effects
- Validation against experimental measurements using traditional formulations

**Droplet Dynamics as the Linchpin of Delivery Optimization**

The present computational framework reveals that droplet dynamics—encompassing velocity, deformation, internal circulation, and interfacial behavior—constitutes the fundamental control variable for optimizing drug delivery in traditional medicine systems. Unlike conventional drug delivery platforms that rely primarily on formulation chemistry, the capillary-based approach modeled here demonstrates that hydrodynamic parameters exert a first-order influence on therapeutic uptake, often outweighing the effects of molecular diffusion alone. This finding carries profound implications for the design of traditional liquid preparations, which have historically been optimized through empirical observation rather than mechanistic understanding.

The inverse proportionality between droplet velocity and total drug dose ($M_{total} \propto 1/u_0$) establishes a clear design principle: slower droplet transit maximizes drug loading. However, this relationship must be interpreted within the broader context of treatment logistics. For a traditional healer preparing a decoction or infusion, the droplet velocity corresponds to the administration rate—whether through oral ingestion, topical application, or instillation. Our results indicate that reducing the delivery rate by an order of magnitude (from 1.0 mm/s to 0.1 mm/s) increases drug loading by approximately 700%, from ~10 mol/m³ to ~71 mol/m³. This suggests that slow, deliberate administration protocols—which may already be embedded in traditional practices through ritualistic or mindful preparation—are not merely culturally significant but scientifically advantageous for maximizing therapeutic dose.

Conversely, the pressure field analysis (Section 3.6) reveals that higher velocities generate substantially larger hydrodynamic stresses. The maximum pressure scales approximately as $P_{max} \propto u_0^{1.8}$, increasing from 3.2 Pa at 0.1 mm/s to 128.5 Pa at 1.0 mm/s. For traditional formulations containing shear-sensitive bioactive compounds—such as polysaccharides, proteins, or vesicular structures—this pressure escalation may induce mechanical degradation, reducing efficacy despite the shorter administration time. The optimization problem thus becomes multi-objective: minimize velocity to maximize dose and preserve compound integrity, while maximize velocity to enhance patient compliance and practical feasibility. The computational framework provides the quantitative basis for navigating this trade-off.

**The Sigmoidal Accumulation Profile: A Design Heuristic for Membrane-Contact Systems**

The S-shaped (sigmoidal) temporal accumulation profile observed in Figure 4 and Figure 9 is not merely a mathematical curiosity but a diagnostic signature of the droplet-membrane interaction dynamics. The three distinct phases—entry (gradual contact growth), steady passage (maximum flux), and exit (diminishing contact)—correspond to specific geometric configurations of the droplet relative to the permeable membrane. For traditional medicine delivery systems, this profile provides actionable insights:

**Phase I (Entry):** The initial slow uptake corresponds to the progressive establishment of droplet-membrane contact. During this phase, the effective contact area increases as the droplet advances over the membrane edge. Formulations with higher surface tension or lower contact angles would experience a steeper entry slope due to enhanced wetting, thereby accelerating the onset of therapeutic uptake. This suggests that traditional preparations could be optimized by adjusting surface-active components—such as natural surfactants present in many plant extracts—to modulate interfacial behavior.

**Phase II (Steady Uptake):** The linear or quasi-linear accumulation during full membrane overlap represents the period of maximum drug influx. The duration of this phase is directly proportional to the membrane length and inversely proportional to droplet velocity ($T_{steady} = L_m / u_0$). For a given membrane geometry, the total dose delivered during this phase can be predicted simply as $M_{steady} = J_0 A_{contact} T_{steady}$, independent of the diffusion coefficient. This simplification is powerful for rapid estimation: if the contact area can be measured or estimated, the delivered dose is determined entirely by the flux boundary condition and residence time.

**Phase III (Exit):** The saturation plateau emerges as the droplet leaves the membrane region. The asymptotic approach to the final concentration is governed by diffusive equilibration within the droplet, with a characteristic time scale $\tau_{diff} \sim R^2 / D$, where R is the droplet radius. For the present parameters (R≈0.5 mm, D = 5 × $10^{-9}$) m²/s), $\tau_{diff} \approx 50$ s—substantially longer than the membrane residence time for most velocities. This implies that significant concentration gradients persist within the droplet after membrane traversal, as confirmed by the entropy analysis (Section 3.7). For traditional formulations containing multiple active compounds, these persistent gradients could lead to spatial segregation of bioactive constituents, potentially affecting the synergistic actions that define many indigenous healing practices. The entropy metric introduced in this study provides a rigorous, thermodynamically grounded measure of this segregation, enabling formulators to design protocols that achieve both high total dose and homogeneous distribution.

**Mixing and Homogenization: The Entropy Perspective**

The entropy-based analysis (Section 3.7) introduces a paradigm shift in how we evaluate drug delivery quality. Traditional metrics focus on total dose or mean concentration, but these fail to capture the spatial uniformity of the therapeutic agent—a critical consideration for polyherbal formulations where synergistic effects depend on balanced constituent ratios. The entropy density $s_{vol}=-c\ln(c/c_{ref})$ provides a natural measure of disorder: a perfectly mixed droplet (uniform concentration) maximizes entropy, while a segregated droplet (steep gradients) minimizes it.

Our results demonstrate that lower droplet velocities yield not only higher total doses but also significantly more homogeneous concentration distributions. At $u_0$=0.1 mm/s, the radial entropy profile at the droplet midplane is broad and relatively flat, indicating near-uniform mixing throughout the volume. At $u_0$=1.0 mm/s, the entropy profile is sharply peaked near the membrane interface, with rapid decay toward the droplet center. This velocity-dependent homogenization arises from the interplay between convective mixing (driven by internal circulation) and diffusive transport. At low velocities, the extended residence time permits internal recirculation cells to redistribute the incoming drug throughout the droplet volume; at high velocities, the drug is advected primarily along the membrane surface before the droplet exits, leaving the core region depleted.

For traditional medicine formulators, this finding has direct practical implications. Many indigenous preparations are administered as single-dose units—a spoonful of decoction, a drop of tincture, or an application of poultice. If the concentration within that dose is spatially heterogeneous, the patient may receive a sub-therapeutic or supra-therapeutic amount depending on which portion of the droplet is administered. Entropy maximization thus becomes a quality control objective: ensure that each volume element of the delivered dose carries a consistent therapeutic load. The computational framework presented here enables the quantitative optimization of preparation parameters (velocity, droplet size, viscosity) to achieve this objective, providing a scientific basis for standardization while respecting traditional preparation methods.

**Formulation Parameters as Optimization Levers**

While the present study focused primarily on droplet velocity as the independent variable, the model's parametric structure enables systematic exploration of other formulation parameters that are directly controllable in traditional medicine preparation. These parameters can be understood through their influence on the dimensionless groups governing droplet dynamics and mass transport:

**Viscosity (μ):** Increasing the viscosity of the aqueous phase (e.g., through the addition of mucilaginous plant extracts) reduces the internal circulation velocity within the droplet, suppressing convective mixing. The Capillary number $Ca = \mu u_0 / \gamma$ quantifies the relative importance of viscous to surface tension forces. For $Ca \ll 1$, surface tension dominates, maintaining a spherical droplet shape; for $Ca \sim 1$, viscous forces deform the droplet, potentially increasing the membrane contact area and enhancing uptake. However, higher viscosity also reduces the diffusion coefficient (through the Stokes-Einstein relation $D = k_B T/(6\pi\mu r)$ for spherical solutes), creating a trade-off. The model can predict the optimal viscosity that balances enhanced contact (via deformation) against reduced molecular mobility.

**Surface Tension (γ):** Natural surfactants present in many plant extracts—saponins, terpenes, and phospholipids—can significantly reduce the surface tension of traditional preparations. Lower surface tension decreases the Laplace pressure ($\Delta P = 2\gamma/R$), facilitating droplet deformation and increasing the contact area with the membrane. The results from the contact angle variation (Equation 3) confirm that interfacial properties directly modulate the pressure distribution and, consequently, the effective flux area. Formulators can leverage this insight by selecting plant materials with high surfactant content or by adding natural emulsifiers to enhance droplet spreading and drug uptake.

Droplet Size (R): The droplet radius enters the transport equations through the diffusion time scale ($\tau_{diff} \sim R^2 / D$) and the capillary pressure ($\Delta P \sim \gamma / R$). Smaller droplets have larger surface-area-to-volume ratios, potentially increasing the flux per unit volume, but they also experience higher internal mixing velocities due to stronger surface tension-driven recirculation. The model can be extended to optimize droplet size for a given membrane geometry and target dose, providing a rational basis for selecting administration devices (e.g., dropper size, nebulizer settings).

**Membrane Permeability ($J_0$):** The flux boundary condition $J_0$ represents the permeability of the biological or device membrane to the therapeutic agent. In traditional medicine, this may correspond to the absorption rate across the oral mucosa, skin, or gastrointestinal epithelium. The linear relationship between total dose and $J_0$ (Equation 7) implies that enhancing membrane permeability is equally effective as increasing residence time—but with the practical distinction that permeability is often formulation-dependent and difficult to modify without altering the therapeutic composition. The model enables sensitivity analysis to determine whether formulation modifications (e.g., adding penetration enhancers) or delivery modifications (e.g., slower administration) are more effective for a given application.

### Multi-Objective Optimization and Pareto Frontiers

The competing objectives identified throughout this discussion—maximize dose, maximize homogeneity, minimize degradation, minimize administration time—naturally lead to a multi-objective optimization formulation. For a given traditional medicine formulation, the Pareto frontier represents the set of non-dominated solutions were improving one objective necessarily degrades another. The computational framework developed here can systematically generate this frontier by sweeping the parameter space and evaluating the trade-offs.

For example, Figure 10 (conceptual) illustrates the trade-off between total dose and delivery time for the present system. Points on the Pareto frontier represent optimal velocity selections: at low velocities, dose is maximized but time is excessive; at high velocities, time is minimized but dose is compromised. The shape of this frontier provides decision-makers—whether traditional healers, clinicians, or patients—with explicit information about the consequences of their choices, enabling informed, culturally appropriate decisions.

The entropy metric further enriches this optimization by adding a quality dimension to the dose-time trade-off. A formulation delivered at moderate velocity may achieve acceptable dose and time while maximizing entropy (spatial homogeneity), representing a balanced solution that respects both therapeutic efficacy and practical constraints. The model can be extended to incorporate weighting factors that reflect the priorities of different stakeholders—for instance, a patient may prioritize convenience (short time), while a healer may prioritize efficacy (high dose and homogeneity). This flexibility makes the framework adaptable to diverse cultural and clinical contexts.

### Integration with Empirical Traditional Knowledge

One of the most significant contributions of this work is its potential to validate and enhance traditional knowledge through mechanistic understanding. Indigenous healing practices have been refined over generations through empirical observation, but the underlying mechanisms often remain implicit. By providing a quantitative, physically grounded explanation for why certain preparation methods work, the computational framework bridges the epistemological gap between traditional and modern science.

Consider, for example, the common traditional practice of slow, gentle heating of herbal decoctions. Our results suggest that slow administration (low droplet velocity) enhances drug uptake by maximizing residence time—a mechanism that parallels the slow extraction of active compounds through gentle heating. Both practices share the principle of extended interaction time between the therapeutic agent and the delivery medium (whether solvent or membrane). The model provides a formal theoretical foundation for this intuitive knowledge, enabling its systematic application to new formulations.

Similarly, the practice of stirring or agitating traditional preparations during administration can be understood through the entropy analysis: agitation enhances internal mixing, promoting homogeneity and reducing concentration gradients. The model quantifies the degree of mixing achieved through convection, providing a benchmark against which empirical stirring protocols can be evaluated. Healers can use this information to determine whether stirring is necessary, and if so, what intensity and duration are optimal.

The integration process must be collaborative and respectful, recognizing that traditional knowledge holders are experts in their own right. The computational framework should be presented not as a replacement for traditional wisdom but as a complementary tool that can:

- Explain why certain practices are effective
- Identify critical control parameters that may be overlooked
- Suggest modifications that preserve the holistic integrity of the preparation
- Provide documentation for regulatory and quality assurance purposes

### Toward Regulatory Integration and Standardization

The global integration of traditional medicine into mainstream healthcare systems requires the development of standardized quality control metrics that are both scientifically rigorous and culturally appropriate. The computational framework presented here offers several quantifiable metrics that can serve this purpose:

- **Total Dose ($M_{total}$):** The absolute amount of therapeutic agent delivered, directly correlated with pharmacological effect.
- **Delivery Efficiency ($\eta = M_{total} / M_{available}$):** The fraction of the available drug that is actually absorbed, providing a measure of formulation performance independent of concentration.
- **Homogeneity Index ($H = -\int s_{vol}\, dV / M_{total}$):** A normalized measure of spatial uniformity, with H=1 for perfect mixing and H=0 for complete segregation.
- **Velocity Sensitivity ($\partial M / \partial u_0$):** A measure of formulation robustness to variations in administration rate, important for real-world conditions where precise flow control may not be possible.
- **Pressure Stress Index ($\Psi = \int |\nabla P|\, dV$):** A measure of the mechanical stress experienced by the formulation, relevant for shear-sensitive compounds.

These metrics can be embedded in regulatory guidelines for traditional medicine products, providing a common language for manufacturers, regulators, and healthcare providers. Importantly, they do not require the abandonment of traditional preparation methods; rather, they offer a framework for documenting and optimizing existing practices within a standardized framework.

The model also enables virtual bioequivalence testing—predicting whether a modified formulation or delivery protocol produces equivalent drug uptake to an established reference. This capability is particularly valuable for scaling up traditional preparations from small-batch artisanal production to larger-scale manufacturing, where maintaining consistency is challenging. By simulating the effects of process variations, the model can identify critical process parameters that must be controlled to ensure product quality.

**Addressing Model Limitations and Future Extensions**
While the current model provides a robust foundation, several limitations must be acknowledged to guide future development and ensure appropriate interpretation of results:

**Single-Component Simplification:** Traditional formulations often contain dozens or hundreds of bioactive compounds, each with distinct diffusion coefficients, membrane permeabilities, and interactions. Extending the model to multi-component transport requires solving coupled convection-diffusion equations with competitive binding and reaction kinetics. Preliminary computational studies suggest that component interactions can significantly alter transport dynamics, with small, highly diffusive molecules potentially facilitating the transport of larger, less mobile compounds through osmotic or convective effects. This synergistic transport may be a key mechanism underlying the enhanced efficacy of polyherbal formulations.

**Constant Flux Assumption:** The membrane flux $J_0$ is treated as spatially and temporally constant, but real biological membranes exhibit nonlinear, time-dependent permeability. Factors such as membrane fouling, concentration polarization, and active transport mechanisms can modulate the effective flux. Future models should incorporate dynamic permeability models informed by experimental data, potentially using the framework of irreversible thermodynamics to capture coupled transport phenomena.

**Geometric Idealization:** The axisymmetric capillary geometry, while computationally efficient, does not capture the complex three-dimensional geometries of real biological systems—branched vascular networks, tortuous mucosal surfaces, or the irregular morphology of inflamed tissues. However, the fundamental scaling relationships established here (e.g., $M \propto 1/u_0$) are expected to hold in more complex geometries if the relevant length scales are appropriately defined. Extending the model to three dimensions, while computationally expensive, would enable patient-specific simulations for personalized medicine applications.

**Non-Newtonian Rheology:** Many traditional formulations—particularly those containing polysaccharides, gums, or suspended particulates—exhibit non-Newtonian behavior, including shear-thinning, yield stress, and viscoelasticity. The present model assumes Newtonian fluid behavior, which may underestimate the complexity of the flow field in real preparations. Incorporating non-Newtonian rheological models (e.g., power-law, Carreau-Yasuda, or Herschel-Bulkley) is a priority for future work, as it would enable the simulation of formulations with realistic flow properties.

**Thermal Effects:** Temperature influences diffusion coefficients (through the Arrhenius relation), viscosity (through the Vogel-Fulcher-Tammann equation), and surface tension. Traditional preparation methods often involve heating or cooling, and the temperature profile during administration may significantly affect drug uptake. Coupling the fluid dynamics and mass transport models with heat transfer equations would provide a more complete description of the system, enabling optimization of thermal protocols.

**Experimental Validation:** The most critical limitation is the absence of experimental validation using real traditional formulations. While the analytical solutions provide internal consistency checks (Section 3.5), direct comparison with experimental measurements of drug uptake in capillary devices is necessary to validate the model's predictive accuracy. Such validation should be conducted using both model compounds (e.g., dyes or synthetic drugs) and authentic traditional formulations (e.g., standardized herbal extracts), with careful documentation of all physicochemical parameters.

**Broader Implications for Healthcare Equity and Indigenous Rights**
The optimization of traditional drug delivery through computational modeling has implications that extend far beyond technical performance. At its core, this work addresses the systemic marginalization of indigenous knowledge systems within the global healthcare framework. By providing scientific validation for traditional practices, the computational framework contributes to:

**Epistemic Justice:** Recognizing that indigenous knowledge is not merely "folk wisdom" but a sophisticated system of empirical observation and rational hypothesis testing, deserving of the same respect accorded to Western scientific knowledge. The model demonstrates that traditional practices—such as slow administration, gentle heating, and stirring—have mechanistic rationales that align with modern pharmaceutical principles. This validation is essential for challenging the historical dismissal of traditional medicine as unscientific or primitive.

**Cultural Continuity:** By enabling the optimization and standardization of traditional preparations, the model supports the continued use of ancestral healing practices in contemporary contexts. Rather than forcing traditional healers to abandon their methods in favor of "modern" alternatives, the framework offers a path toward culturally appropriate innovation that respects and enhances existing knowledge.

**Regulatory Recognition:** The standardized metrics provided by the model (Section 4.7) can facilitate the regulatory approval of traditional medicines, enabling their integration into national health systems. This is particularly important in countries where traditional medicine is the primary or only healthcare option for rural and marginalized populations. By providing a scientific basis for quality control, the model supports the safe and effective use of traditional medicines without imposing Western-centric standards that may be inappropriate or inaccessible.

**Economic Empowerment:** The commercialization of traditional medicines, when done ethically and with community consent, can provide economic benefits to indigenous communities. The computational framework can support this process by enabling the rational design of formulations that meet regulatory standards, facilitating market access while preserving the intellectual property rights of traditional knowledge holders.

**Global Health Equity:** Ultimately, the integration of optimized traditional medicines into global healthcare could expand access to affordable, culturally acceptable treatments for billions of people. The computational framework presented here is a step toward this vision, demonstrating that modern science and ancestral wisdom can coexist and reinforce each other in the service of human health and well-being.

**Constructal Theory Application in Droplet-Based Drug Delivery**

The constructal theory, first articulated by Bejan (1997), posits that flow systems—whether natural or engineered—evolve over time to facilitate greater access for their currents, developing architectures that minimize resistance to flow. This principle, originally formulated for thermodynamic and fluid systems, finds profound application in the present study of droplet-based drug delivery, offering a unifying framework that connects the observed hydrodynamic optima, the spatial organization of concentration fields, and the fundamental design principles governing efficient therapeutic transport.

**Constructal Design as a Unifying Principle for Drug Delivery Optimization**

The inverse relationship between droplet velocity and total drug dose ($M_{total} \propto 1/u_0$) can be reinterpreted through the constructal lens as a manifestation of the flow resistance-access trade-off. In constructal theory, the flow architecture that emerges—whether a river basin, a vascular network, or, in this case, a moving droplet—represents the configuration that maximizes access while minimizing the resistance to the imposed currents. For the droplet traversing the permeable membrane, the fundamental currents are the drug molecules diffusing from the membrane into the droplet interior. The resistance to these currents is governed by the convective time scale ($\tau_{conv}=L_m/u_0$) relative to the diffusive time scale ($\tau_{diff}=R^2/D$). The constructal optimum corresponds to the velocity that balances these two-time scales, ensuring that the drug molecules have sufficient time to penetrate the droplet volume without inducing excessive hydrodynamic stresses.

The present results demonstrate that the system naturally selects slower velocities as constructally more efficient for maximizing drug uptake, because the reduced flow resistance (lower pressure gradients, as shown in Table 2) facilitates enhanced molecular access to the droplet interior. This is consistent with the constructal principle that the flow architecture evolves to minimize global flow resistance, which in this context corresponds to the dimensionless parameter:

$$\widehat{M} = \frac{M_{total}}{J_0 A_{contact} L_m / D} = \frac{D}{u_0 R} \sim \frac{1}{Pe} \qquad (14)$$

where Pe = $u_0$ R/D is the Péclet number. The inverse dependence on the Péclet number reveals that the constructal design of the droplet-membrane system is governed by the competition between convection and diffusion, a central theme in constructal theory applied to mass transport.

**The Entropy-Maximizing Configuration: Constructal Homogenization**

The entropy analysis presented in Section 3.7 provides a particularly compelling illustration of constructal theory in action. The constructal principle states that flow systems evolve to generate architectures that distribute imperfection optimally, maximizing global performance while allowing local irreversibilities. In the context of drug delivery, the entropy density ($s_{vol}$ = -cln($c/c_{ref}$)) represents a measure of local mixing imperfection—low entropy regions correspond to ordered, poorly mixed states, while high entropy regions represent well-mixed, disordered configurations.

The radial profiles of weighted entropy density (Figure 8c) reveal that the system spontaneously organizes its internal flow to maximize entropy generation, subject to the constraints imposed by the droplet velocity and geometry. At low velocities ($u_0$ = 0.1 mm/s), the entropy profile is broad and flat, indicating that the system has achieved a near-uniform configuration—the constructal optimum for homogenization. At high velocities ($u_0$=1.0 mm/s), the entropy profile is sharply peaked near the membrane interface, indicating that the system has not had sufficient time to redistribute the incoming drug throughout the volume.

**This Observation can be Formalized Through the Constructal Statement**

The droplet-flow configuration evolves (subject to constraints of fixed volume, velocity, and membrane permeability) to maximize the cumulative entropy generation over the delivery interval, which equivalently minimizes the global concentration heterogeneity.

Mathematically, this is expressed as:

$$S_{gen} = \int_V \frac{k}{T^2}|\nabla T|^2 dV + \int_V \frac{\Phi\mu}{T} dV + \int_V \frac{R}{c}|\nabla c|^2 dV \tag{15}$$

where the third term represents the entropy generation due to mass diffusion. The constructal optimum corresponds to the velocity that maximizes the global entropy generation rate, subject to the fixed droplet volume and the imposed flux boundary condition. The present results indicate that this optimum occurs at velocities below 0.2 mm/s, where the system has sufficient time to develop its internal architecture.

**Hierarchical Constructal Design: From Droplet to Membrane to Capillary**

The constructal principle is inherently hierarchical: flow architectures evolve at multiple scales, from the molecular to the macroscopic. The present framework can be extended to consider the constructal optimization at three distinct levels:

**Level 1: Molecular Architecture (Drug-Molecule Scale)**

At the smallest scale, the constructal design corresponds to the molecular structure of the drug molecules themselves. Traditional medicine formulations often contain complex molecular architectures—polyphenols, terpenes, alkaloids—that have evolved or been selected for optimal transport properties. The constructal principle predicts that these molecular architectures are shaped by the same flow-access imperative: they minimize the resistance to molecular diffusion through biological barriers. The diffusion coefficient D = $5\times10^{-9}$ $m^2/s$ used in this study represents the aggregated effect of these molecular-level constructal designs.

**Level 2: Droplet Architecture (Droplet Scale)**

At the intermediate scale, the droplet shape and internal circulation patterns represent the constructal architecture that optimizes the balance between convective transport (controlled by droplet velocity and internal recirculation) and diffusive penetration (controlled by the diffusion coefficient) . The present results demonstrate that the droplet naturally deforms under the influence of surface tension and shear forces to achieve a shape that maximizes the membrane contact area (and thus the flux) while minimizing the internal resistance to mixing. The contact angle dynamics modeled in Equation (3) represent a form of constructal wetting, where the system configures its interfacial geometry to minimize the global flow resistance.

**Level 3: Capillary-Membrane Architecture (System Scale)**

At the largest scale, the overall geometry of the capillary system—the placement of the permeable membrane, the droplet size relative to the capillary radius, and the flow path—represents the constructal design that minimizes the total resistance to drug delivery. The present model's axisymmetric geometry and boundary conditions (Section 2.1) represent a specific instantiation of this system-level constructal design. The optimal placement of the membrane at z=0.6-0.8 mm, with the abrupt contact angle transition, creates a local flow environment that balances access (the droplet must traverse the membrane) with resistance (the droplet must maintain integrity while being sheared).

The hierarchical nature of this constructal design implies that optimization at one scale influences the achievable performance at other scales. For example, the molecular-level diffusion coefficient (D) sets the characteristic time scale for droplet-level mixing ($\tau_{diff}$~$R^2$/D), which in turn determines the optimal system-level velocity. This multi-scale coupling is a hallmark of constructal theory and underscores the need for integrated optimization strategies in traditional medicine formulation design.

**Time-Dependent Constructal Evolution: The S-Shaped Accumulation Curve as a Constructal Signature**

The S-shaped (sigmoidal) temporal accumulation profile (Figures 4 and 9) can be interpreted as the constructal evolution of the droplet-membrane system as it traverses the three distinct phases of contact: entry, steady passage, and exit. This temporal signature reflects the system's ongoing adaptation to the changing boundary conditions, representing a dynamic constructal optimization process.

**Phase I (Entry):** As the droplet first encounters the membrane, the contact area increases progressively. The constructal response is to rapidly reconfigure the internal flow field to accommodate the new influx of drug molecules. This is reflected in the initial gradual slope of the accumulation curve, which corresponds to the development of the high-entropy mixing zones near the membrane interface (Figure 8a).

**Phase II (Steady Passage):** During the period of full membrane overlap, the system has achieved a quasi-steady constructal architecture that balances the incoming flux with the internal transport. The near-linear accumulation during this phase indicates that the system has reached a constructal equilibrium, where the global flow resistance is minimized for the given constraints.

**Phase III (Exit):** As the droplet leaves the membrane, the constructal architecture must adapt to the cessation of the influx. The gradual approach to the saturation plateau represents the system's relaxation to a final constructal state, with the remaining concentration gradients slowly eroding through diffusive transport.
The mathematical expression for this temporal constructal evolution can be approximated by the sigmoidal function:

$$M(t) = \frac{M_{max}}{1+exp[-k(t-t_0)]} \tag{16}$$

where $M_{max}$ is the final delivered dose, k is the constructal growth rate (which depends on the velocity and diffusion coefficient), and $t_0$ is the time of maximum slope (corresponding to the midpoint of membrane traversal). The constructal growth rate k can be interpreted as the rate of architectural optimization, indicating how quickly the system reorganizes its internal flow structure to maximize drug uptake. For the present parameters, k is inversely proportional to the droplet velocity, confirming that slower velocities allow more complete constructal evolution.

**Constructal Optimization of Traditional Medicine Formulations**
The constructal framework offers a systematic methodology for optimizing traditional medicine formulations that is both scientifically rigorous and culturally respectful. Rather than imposing an external optimization objective (e.g., "maximize dose at all costs"), the constructal approach recognizes that the system itself reveals the optimal architecture through its response to the governing physics. The practitioner's role is to identify the constructal parameters that lead to the desired performance and to adjust the controllable variables accordingly.

For traditional medicine formulators, this implies Identify the constructal constraints. The fixed constraints of the system—droplet volume, capillary radius, membrane permeability, diffusion coefficient—define the design space within which constructal optimization can occur. These constraints are largely determined by the traditional preparation method and the biological delivery route.

Measure the constructal response. By systematically varying the controllable parameters (droplet velocity, viscosity, surface tension) and observing the resulting constructal performance metrics (dose, homogeneity, pressure stress), the formulator can map the constructal landscape of their formulation.

Identify the constructal optimum. The constructal optimum corresponds to the parameter set that yields the most favorable balance of performance metrics, as determined by the constructal principle of maximizing access while minimizing resistance. For the present system, this optimum occurs at velocities below 0.2 mm/s, where both total dose and homogeneity are maximized.

Validate through constructal benchmarking. The constructal performance of a new formulation or delivery protocol can be benchmarked against established reference systems, providing a quantitative basis for quality control and regulatory approval.

The constructal perspective also offers a unifying language for communicating between traditional healers and modern scientists. Concepts such as "slower administration enhances absorption" or "stirring promotes even distribution" can be formalized as constructal statements about flow architecture optimization, bridging the conceptual gap between empirical wisdom and mechanistic understanding.

**Integration with Traditional Knowledge: Constructal Wisdom in Ancestral Practices**
Perhaps the most profound application of constructal theory in the present context is its ability to validate and explain traditional knowledge through a fundamental physical principle. Indigenous healing practices have long recognized the importance of slow, gentle administration—the constructal principle provides the scientific rationale for this wisdom.

**Consider the Following Examples**
**Slow Infusion:** Traditional healers often recommend that herbal decoctions be consumed slowly, allowing the active compounds to be absorbed gradually. The constructal framework reveals that this practice maximizes the membrane residence time, corresponding to the leftmost point in Figure 5 where the dose is maximized. The reduced velocity decreases the Péclet number, enhancing diffusive penetration and homogenization (Figure 8c).

**Gentle Stirring:** Many traditional preparations are stirred or agitated during administration. The entropy analysis (Section 3.7) demonstrates that internal mixing enhances homogeneity, which constructal theory interprets as the system spontaneously developing architectures that maximize entropy generation and minimize concentration gradients. Stirring effectively accelerates the constructal evolution of the internal flow field.

**Temperature Control:** Traditional practices often emphasize the importance of temperature—avoiding excessive heat that might degrade active compounds, or applying warm preparations to enhance absorption. The constructal framework can be extended to include thermal effects, where the thermal diffusion time scale $\tau_{therm} \sim R^2/\alpha$ interacts with the mass diffusion time scale to determine the overall constructal optimum.

By providing a physically grounded explanation for these practices, the constructal framework validates traditional knowledge as a form of sophisticated, empirically-derived constructal optimization. This validation is essential for epistemic justice and for the ethical integration of traditional medicine into global healthcare systems.

**Future Directions: Constructal Design of Multi-Scale Drug Delivery Systems**
The application of constructal theory to the present study opens several promising avenues for future research:

**Multi-Component Constructal Optimization:** Traditional formulations contain multiple bioactive compounds with different diffusion coefficients and membrane permeabilities. The constructal principle predicts that the system will develop architectures that optimize the simultaneous transport of multiple components, potentially leading to preferential enrichment of the most therapeutically active compounds. This can be modeled by extending Equation (15) to include multiple species with coupled entropy generation.

**Constructal Design of Delivery Devices:** The capillary geometry used in the present study represents a simplified constructal architecture. Future work could apply constructal theory to the design of actual delivery devices—such as inhalers, droppers, or transdermal patches—that are specifically optimized for traditional medicine formulations.

**Constructal Networks for Systemic Delivery:** For formulations that require systemic circulation (e.g., oral or intravenous delivery), the constructal principle can be applied to the vascular network, optimizing the distribution of drug-loaded droplets to target tissues. This would extend the framework to include the constructal architecture of the entire cardiovascular system.

**Constructal Adaptation to Patient Variability:** The constructal optimum for drug delivery may vary between patients due to differences in physiology, disease state, or genetic factors. Future models could incorporate personalized constructal optimization, where the delivery parameters are tailored to the individual patient's constructal response.

**Conclusion: Constructal Theory as a Bridge Between Tradition and Innovation**
The integration of constructal theory with the computational fluid dynamics framework developed in this study represents a significant advance in the rational design of traditional medicine delivery systems. By providing a fundamental physical principle that governs the evolution of flow architectures, constructal theory offers:

- **A Unifying Framework** that connects the molecular, droplet, and system scales, enabling integrated optimization across multiple levels of organization.
- **A Scientific Rationale** for traditional practices, validating ancestral knowledge as sophisticated constructal optimization.
- **A Quantitative Methodology** for optimizing formulation parameters, moving beyond trial-and-error to predictive, principle-based design.
- **A Respectful Language** for communication between traditional healers and modern scientists, bridging epistemological divides.

The constructal principle—that flow systems evolve to maximize access while minimizing resistance—provides a powerful lens through which to view the present results. The inverse relationship between velocity and dose, the S-shaped accumulation profile, and the entropy-maximizing mixing patterns all emerge as manifestations of this fundamental principle. By embracing constructal theory, the field of traditional medicine formulation can move toward a future where ancestral wisdom and modern science converge, guided by the shared principle of efficient, equitable, and holistic therapeutic delivery.

## Conclusion

This study establishes a high-fidelity computational fluid dynamics framework to quantitatively characterize the transport phenomena governing therapeutic uptake in a capillary-based droplet delivery system, directly addressing a critical gap in the rational design of traditional medicine formulations. By integrating axisymmetric two-phase flow, moving mesh interface tracking, and diluted species transport, the model successfully resolves the complex interplay between hydrodynamics, interfacial forces, and mass transfer, providing a mechanistic understanding of drug delivery dynamics that has been previously inaccessible through empirical approaches alone.

The parametric analysis yields several definitive conclusions. First, the total absorbed drug dose scales inversely with droplet velocity ($M_{total} \propto 1/u_0$), a direct consequence of the membrane residence time that is validated with a correlation coefficient $R^2 > 0.99$ against analytical solutions. This relationship establishes a quantitative design rule: reducing droplet velocity from 1.0 mm/s to 0.1 mm/s increases the mean drug concentration nearly sevenfold (from ~10 mol/m³ to ~71 mol/m³), demonstrating the profound impact of delivery kinetics on therapeutic loading. Second, the temporal accumulation follows a distinctive sigmoidal profile, governed by the progressive development of the droplet–membrane contact area during entry and exit, with the early-stage diffusion scaling precisely as $t^{3/2}$, confirming the correct implementation of the convection–diffusion physics. Third, the pressure field analysis reveals localized perturbations of approximately 3 Pa/mm at the membrane boundaries due to abrupt contact angle transitions, highlighting the critical role of surface wetting dynamics in modulating droplet deformation and, consequently, the effective flux area.

Beyond bulk dose prediction, the entropy-based mixing analysis introduces a thermodynamic measure of spatial homogeneity that is particularly relevant to traditional polyherbal formulations, which rely on the synergistic action of multiple bioactive compounds. The results demonstrate that lower velocities (e.g., 0.1 mm/s) not only maximize total drug loading but also produce significantly broader and more uniform entropy distributions across the droplet volume, indicating enhanced internal mixing and homogenization. This finding is crucial, as a heterogeneous concentration field could lead to inconsistent dosing upon administration, whereas a well-mixed droplet ensures that each volume element carries a balanced therapeutic load—a principle that aligns intrinsically with the holistic philosophy of indigenous healing practices.

From a translational perspective, this computational framework empowers traditional healers and formulation scientists to move beyond empirical trial-and-error, offering a predictive tool to optimize preparation parameters—such as flow rate, droplet size, fluid viscosity, and surface tension—while preserving the integrity of ancestral knowledge. By enabling the systematic evaluation of delivery efficiency and spatial uniformity, the model provides a scientific basis for establishing standardized quality control metrics, which are essential for regulatory acceptance and the ethical global integration of traditional medicines. Importantly, this work demonstrates that computational modeling need not supplant traditional practices; rather, it offers a means to validate, enhance, and respectfully modernize them through mechanistic understanding.

While the current model provides a robust foundation, several limitations warrant acknowledgment and motivate future investigations. The assumption of single-component diffusion and constant flux boundary conditions represents an idealization, and subsequent work must extend this framework to include multi-component competitive transport, non-Newtonian rheology characteristic of herbal decoctions and suspensions, and coupled thermal-fluid effects that influence diffusion coefficients and viscosity. Furthermore, the idealized axisymmetric geometry should be expanded to three-dimensional physiological configurations, such as branched vascular networks or mucosal surfaces, to enhance clinical relevance. Critically, experimental validation using model traditional formulations—such as standardised herbal extracts—remains a pivotal next step to translate these in silico predictions into clinically actionable guidelines.

In conclusion, this work represents a paradigm shift in the convergence of ancestral healing knowledge and modern pharmaceutical engineering. It provides a scientifically rigorous, thermodynamically grounded foundation for the evidence-based optimization of traditional medicine delivery systems, promoting culturally appropriate healthcare innovation while upholding the holistic principles that define these ancient practices. By bridging empirical wisdom with predictive computational science, this framework ultimately contributes to the global goal of equitable, accessible, and patient-centered healthcare for all communities—honoring the past while forging a rational, data-driven path toward the future.

## References


1. World Health Organization. (2023). Traditional, complementary and integrative medicine. Geneva: WHO.
2. Rosas-Jiménez, C. A. (2025). The term "Western medicine": An overgeneralization that neglects traditional indigenous healing practices. McGill Journal of Global Health, 14(1), 49–50.
3. Indigenous Healing and Traditional Medicine Working Group. (2026). Principles for the ethical integration of indigenous healing knowledge in contemporary healthcare. Center for Traditional Medicine.
4. Liu, X., et al. (2025). Integrating traditional medicine with modern drug delivery systems: A review of Ayurvedic principles and advanced pharmaceutical technologies. Indian Journal of Ayurveda and Integrative Medicine, 6(2), 45–62.
5. Zhang, W., et al. (2025). Collision of Chinese medicine and materials science: Interdisciplinary biomaterials perspectives. Advanced Materials, 37(15), 2405678.
6. Jalalpure, S. S. (2025). Integrating traditional medicine with modern drug delivery systems: A path forward for holistic health care. Indian Journal of Ayurveda and Integrative Medicine, 6(1), 1–3.
7. Wang, H., & Li, Q. (2025). From forgotten to frontier: Vindicating Latin America's indigenous biotechnology. Journal of Ethnobiology and Ethnomedicine, 21(1), 34–52.
8. Smith, J., et al. (2024). Computational modeling of multiphase flow in microfluidic drug delivery devices. Journal of Computational Physics, 498, 112678.
9. Jamalabadi, M. Y. A., DaqiqShirazi, M., Kosar, A., & Shadloo, M. S. (2017). Effect of injection angle, density ratio, and viscosity on droplet formation in a microfluidic T-junction. Theoretical and Applied Mechanics Letters, 7(4), 243–251.
10. Salmanipour, S., Sokhansanj, A., Jafari, N., Hamishehkar, H., & Saha, S. C. (2025). Numerical investigation to improve pulmonary drug delivery via dry powder inhalers: A review of in-silico modeling. Pharmaceutical Research, 42(8), 1251–1283.
11. Hussain, M., & Zhang, T. (2025). Numerical analysis of droplet formation in T-junction microchannel at low Weber

and Capillary numbers. Microfluidics and Nanofluidics, 29(4), 56–72.
12. Kumar, A., & Singh, R. (2025). CFD approaches in microfluidics for the development of polymeric, lipid-based and inorganic nanoparticles for drug delivery. Chemical Engineering Journal Advances, 19, 100478.
13. Viswanathan, R., & Chen, L. (2025). CFD study and experimental verification of droplet formation characteristics in a flow-focusing microfluidic device. Chemical Engineering Science, 305, 120345.
14. Vishnumurthy, P., Radulesco, T., Bouchet, G., Regard, A., & Michel, J. (2025). Computational fluid dynamics approach for direct nose-to-brain drug delivery: A systematic review and meta-analysis. Journal of Personalized Medicine, 15(10), 447.
15. Ali, M., & Khan, S. (2025). Multiphase CFD modeling of alumina nanoparticle drug delivery in bifurcated coronary arteries with stenosis, aneurysm, and bypass conditions. ScienceDirect. [Advance online publication].
16. Chen, Y., & Wang, L. (2025). Computational fluid dynamics modeling and simulation of nanoparticle-tumor interaction: Systematic literature review. Computational and Structural Biotechnology Journal, 29, 328–352.
17. Yang, F., & Liu, M. (2025). Size control of lipid nanoparticles via simulation-based design of a microfluidic chip and its effect on mRNA delivery in vitro and in vivo. Drug Delivery and Translational Research, 15(8), 2451–2468.
18. Gao, Y., et al. (2022). Machine learning optimization of traditional Chinese medicine compound delivery. Frontiers in Pharmacology, 13, 897654.
19. He, X., Song, Z., Yang, Y., Wu, S., Meng, S., E, H., Li, H., & Ding, G. (2025). Compatibility optimization of the traditional Chinese medicines "Eczema mixture" based on back-propagation artificial neural network and non-dominated sorting genetic algorithm. Frontiers in Pharmacology, 16. [Article number pending].
20. Wu, Z., Wang, Z., Chang, X., et al. (2025). Prioritizing pathway signature using deep learning approach: A novel strategy for traditional Chinese medicine formula generation and optimization. Briefings in Bioinformatics, 26(4), bbaf403.
21. Shivakumar, S. P., et al. (2025). Magneto-radiative modelling and artificial neural network optimization of biofluid flow in a stenosed arterial domain. arXiv:2507.06273.
22. Sharma, P., & Patel, D. (2025). In silico studies of fluid flow, digestion of food and drug dissolution in human stomach. Computers in Biology and Medicine, 180, 108945.